2.2 THE EFFECTS OF VEGETATION DENSITY ON TURBULENT STRUCTURES WITHIN CANOPY SUBLAYER

Jing Huang[1 *], Cassiani Massimo[1], John D. Albertson[1 2]
[1] Department of Civil and Environmental Engineering, Duke University, Durham, North Carolina
[2] Nicholas school of the Environment, Duke University, Durham, North Carolina

1 ABSTRACT

Over 30 percent of the earth's land surface is covered by woodland, with the leaf area index (LAI) values ranging approximately from 0.4 to 13. This highly varied vegetation density has significant effects on the turbulent dynamics within and just above plant canopies. The effects of vegetation density on the large-scale coherent structures are investigated in this study through applying the proper orthogonal decomposition (POD) technique on numerically simulated canopy sublayer (CSL). It was found that the inflections on the mean streamwise velocity profile as well as the one-dimensional eigenfunctions obtained from the POD are gradually weakened as the canopy becomes sparser, and almost disappear under the case of the extreme sparse canopy (ESC, LAI=0.0625), resembling that of an atmospheric boundary layer (ABL). The convergence rate of the eigenvalues, which indicates the relative importance of the coherent structures, remains approximately the same for all simulations with different vegetation densities. Multi-dimensional POD analysis demonstrates that the counter-rotating vortices and the strong sweep motion between the vortex pair appear as the dominant structure in the spanwise-vertical plane of CSL, which is in good agreement with precedent results discovered in wind-tunnel experiments. In the spanwise direction, the vortex inclines at the ground with a tilt angle of approximately 45^{o}, consisted with the result in the ABL. In the streamwise direction, the center of the vortex is found to curve up with the maximum orientation angle around 84^{o}. The coherent structures in CSL with higher vegetation density are systematically more elevated.

2 INTRODUCTION

The large-scale coherent structures of turbulent flows within and just above vegetation canopies (canopy sublayer, or CSL) have been under investigation for the past few decades. These organized motions are found to be responsible for the majority of mass and momentum transport at the canopy-atmosphere interface (e.g. Raupach 1981; Gao et al. 1989; Katul et al. 1997; Finnigan and Shaw 2000; Thomas and Foken 2007). Raupach et al. (1996) proposed a theoretical framework to explain most of the significant characteristics of the canopy turbulence on the basis of the plane mixing layer (PML) analogy. However, despite the overall satisfactory description for CSL with 'sufficiently high' vegetation density, noticeable dependences of turbulent structures upon canopy density have been observed (e.g. Novak et al. 2000; Poggi et al. 2004). Provided that terrestrial ecosystems cover a very broad range of vegetation densities (Asner et al. 2003), it is important to quantitatively understand how these structures change as a function of vegetation density.

The overall behaviors of turbulence within CSL vary significantly from those in the surface layer (SL) (Finnigan 2000) and these differences are characterized by: (1) vertically inflected streamwise mean velocity; (2) inhomogeneous second moment profile with height and large skewness and kurtosis; (3) domination of sweeps over ejections in momentum transport (Finnigan 2000). The achieved knowledge on the connections between turbulent flows within the CSL, the atmospheric boundary layer (ABL) and the PML foreshow that large eddies within these three types of flows should be related in a certain way. Huang et al. examined large-scale coherent eddies, resulting from large-eddy simulation (LES) of the ABL, through the use of the proper orthogonal decomposition (POD) technique (Lumley 1967; Lumley 1970; Lumley 1981). The educed dominant structure captures over 30 percent of the total turbulent kinetic energy (TKE) in the near-wall region. Multi-dimensional analysis reveals that coherent eddies are composed of a pair of streamwise counter-rotating vortices and a strong ejection motion between the vortex pair, which is a major contributor to momentum transport. The vortices are found to be inclined in the spanwise direction and curve up in the streamwise direction. Similar analysis performed on a PML confirms the existence of streamwise vortex pair and the significance of these structures in carrying TKE (Delville et al. 1999). Within CSL, large-scale structures are delineated as weak ejections followed by strong sweeps in the streamwise-vertical plane; in the spanwise-vertical plane these structures also consist of a pair of counter-rotating streamwise vortices centered above the canopy and take large fraction of the total TKE (Finnigan and Shaw 2000). However, it is still unclear how these characteristic structures differ as the canopy ranges from sparse to dense.

Here a LES experiment is performed to systematically examine the effects of vegetation density on basic flow statistics as well as the large-scale

* *Corresponding author address:* Department of Civil and Environmental Engineering, Duke University, Durham, North Carolina 27708-0287; e-mail: jing.huang@duke.edu

coherent structures within CSL. The POD technique is applied to identify these characteristic structures from the simulated turbulent flow fileds. The results of turbulent structures computed from the LES are compared with those obtained through an analysis of wind-tunnel experimental data (Finnigan and Shaw 2000).

The present paper is organized as follows. In Section 3, the necessary background knowledge of LES and POD are briefly introduced. In Section 4.1, we compare the basic flow statistics of our LES with preceding results through wind tunnel and flume experiments. In Section 4.2 and 4.3, one-, two- and three-dimensional coherent structures are examined and the effects of vegetation density are investigated. Finally the conclusions are drawn in Section 5.

3 METHODOLOGY

3.1 *The Large-Eddy Simulation*

Currently, LES is the state-of-the-art computational tool for investigating the structure of turbulence in a wide variety of settings, including plant canopies. Its use for modeling the ABL dates back to the work of Deardorff (1972) and since then, developments in LES have proliferated (e.g. Moeng 1984; Schmidt and Schumann 1989; Mason and Thomson 1992; Sullivan et al. 1996; Kosovic 1997; Porte-Agel et al. 2000).

The use of LES as a tool to investigate turbulent flows inside and above forested canopies has rapidly expanded since the work of Shaw and Schumann (1992) as evidenced by the large-number of studies thus far (e.g. Dwyer et al. 1997; Shen and Leclerc 1997; Su et al. 1998; Su et al. 2000; Albertson et al. 2001; Patton et al. 2001; Yang et al. 2006a; Yang et al. 2006b). A modified version of the LES code described in Albtertson (1996) and Albertson and Parlange (1999b; 1999a) is used in this paper. For a detailed description of the equations, the SGS model, boundary conditions and numerical schemes involved, the readers are directed to Cassiani et al. (2008) and the references therein.

The simulations are performed on two nested computational staggered grids: the outer (or coarse) one has 64×32×41 nodes over a domain 1257*m*×628*m*×400*m* that covers what can be considered a neutrally stratified boundary layer; the nested (or refined) grid covers a domain close to the surface 1257*m*×628*m*×80*m* with 256×128×41 nodes. A 25*m* tall forest homogeneously covers the whole horizontal domain. The forest has been simulated as a distributed drag force extending vertically 3 nodes for the coarse-grid simulations and 13 nodes for the nested grid simulations. This configuration gives an aspect ratio between the horizontal and vertical spacing (Δ_x/Δ_z, Δ_y/Δ_z) of about 2 for the coarse grid and 2.5 for the refined grid. The roughness length of the ground surface was set as z_o=0.05*m*. This roughness length is of significance only when the canopy density becomes very low. In general the important sink of momentum is in the upper layers of the canopy and it is explicitly resolved by the drag force.

In our simulations, canopy density is quantified by leaf area index (LAI), which is defined as:

$$LAI(x,y)=\int_0^h a(x,y,z)dz \quad (1)$$

where h is the canopy height and $a(x,y,z)$ is local leaf area density, i.e. area of plant surface for unit volume of space. Since the simulated canopy is horizontally homogeneous, (1) can be shortened as:

$$LAI=\int_0^h a(z)dz\,, \quad (2)$$

where $a(z)$ represents the vertical leaf area density distribution, which basically depicts the vertical shape of canopy. In this study, a canopy with uniform vertical density is simulated with the upper part smoothly decreasing to zero, damping abrupt changes of turbulent variables around canopy top. The dimensionless leaf area density scaled with the LAI is shown in Fig. 1. The canopy density is a crucial parameter in modeling the drag-force term (see Shaw and Schumann 1992; Cassiani et al. 2008):

$$F_i=-C_d a|\overline{\mathbf{u}}|u_i\,, \quad (3)$$

where C_d is an isotropic drag coefficient taken as 0.2 in this study following Katul and Albertson (1998). Indices and meteorological notations are used interchangeably throughout this paper, i.e., the streamwise, spanwise, and vertical directions are $i(=1,2,3)$, or (x,y,z), respectively.

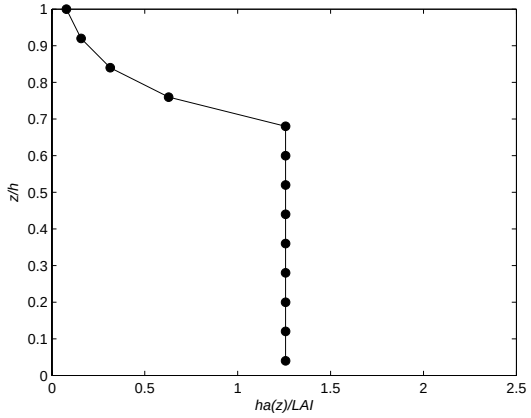

Fig. 1 Vertical distribution of the normalized local leaf area density used in this study

Five LES runs have been performed with LAI=0.0625, 0.25, 1, 4, 16 respectively simulating extremely sparse canopy (ESC), very sparse canopy (VSC), slightly sparse canopy (SSC), slightly dense canopy (SDC), very dense canopy (VDC). We recognize that the cases of ESC, VSC and VDC are either unrepresentative or unrealistic in nature but we hope that the investigation of these cases can help drawing a continuous picture revealing how the turbulent dynamics transit from a boundary-layer-like flow to a mixing-layer-like one.

3.2 *The Proper Orthogonal Decomposition*

The POD was originally introduced into the study of turbulence by Lumley (1967; 1970; 1981). Comprehensive reviews can be found in Holmes et al. (1996), Berkooz et al. (1993) and Sirovich (1987a; 1987b; 1987c). It is briefly presented here for completeness.

Let $u_i(z)$ denote an ensemble of the vertical profile of a turbulent velocity field at an arbitrary (x, y, t) on a finite vertical domain H, which can be part of or the total vertical range of the CSL. The central objective of POD analysis is to decompose an ensemble of realizations of $u_i(z)$ into a sequence of orthogonal functions, which are optimal in the sense of capturing as much the total TKE as possible in a finite number of functions. This constraint is equivalent to solving an eigenvalue problem based on the two-point correlation tensor,

$$\int_H R_{ij}(z,\tilde{z})\phi_j(\tilde{z})d\tilde{z} = \lambda\phi_i(z), \quad (4)$$

where the correlation tensor $R_{ij}(z,\tilde{z}) = \langle u_i(z)u_j(\tilde{z})\rangle$ and $\langle\ \rangle$ represents an ensemble average over x, y and t for one-dimensional analysis. For discrete implementations, the number of the solutions is proportional to the size of $R_{ij}(z,\tilde{z})$, i.e., the grid number in the direction of integration. In order to distinguish between different solutions, an index number m is added such that an eigenfunction can be represented as $\phi_i^{(m)}$ and the associated eigenvalue is then $\lambda^{(m)}$. The amplitude of $\lambda^{(m)}$ indicates the relative importance of the corresponding eigenfunction $\phi_i^{(m)}$. The eigenfunctions are orthogonal and a normalization condition can be imposed so that,

$$\int_H \phi_i^{(m)}(z)\phi_i^{(n)*}(z)dz = \delta_{mn}, \quad (5)$$

where * denotes the complex conjugate. Note that * can be dropped for the current application of one-dimensional analysis because $u_i(z)$ are generally real; however, operations of complex numbers will be involved in multi-dimensional analysis. The original velocity field can be reconstructed by superposing the eigenfunctions,

$$u_i(z) = \sum_n a_n\phi_i^{(n)}(z), \quad (6)$$

where the coefficients a_n are defined as,

$$a_n = \int_H u_i(z)\phi_i^{(n)*}(z)dz. \quad (7)$$

The coefficients of different order are uncorrelated:

$$\langle a_m a_n^*\rangle = \delta_{mn}\lambda^{(n)}. \quad (8)$$

A direct consequence of (8) is that the contribution of eigenfunctions $\phi_i^{(n)}(z)$ to the total TKE is determined by $\lambda^{(n)}$,

$$E = \int_H \langle u_i u_i\rangle dz = \sum_n \lambda^{(n)}. \quad (9)$$

With $\lambda^{(1)} \geq \lambda^{(2)} \ldots \geq \lambda^{(n)}$, the mode associated with the first eigenvalue contributes the most to the TKE, and then the second, and so on. In this paper, the first mode will be generally referred to as the large-scale coherent structure in the one- and multi-dimensional analysis. Due to the existence of homogeneous direction in our simulations, the multi-dimensional POD analysis must be conducted with the assistance of the shot-noise expansion and phase determination techniques (see Moin and Moser 1989; Finnigan and Shaw 2000).

4 RESULTS AND DISCUSSION

4.1 *Flow statistics*

A family portrait of single point turbulent flow statistics obtained from our simulations is presented in Fig. 2, and compared with the experimental measurement in a wind tunnel (Brunet et al. 1994) and a flume (Poggi et al. 2004). This comparison serves as the first test of the LES capability to produce realistic dynamics over horizontally homogeneous canopy of different density. The compared statistical variables include: (a) streamwise mean velocity $\langle u\rangle_{xyt}$, scaled by its value at the canopy top ($u^h = \langle u\rangle_{xyt}|_{z=h}$), where $\langle\ \rangle_{xyt}$ represents the operation of averaging over the horizontal plane and time, and h is the canopy height; (b) opposite of the mean stress $-\langle u'w'\rangle_{xyt}$, where the turbulent velocities are defined as $u_i' = u_i - \langle u\rangle_{xy}$, scaled by the square of the friction velocity, which is defined as $u_* = \sqrt{-\langle u'w'\rangle_{xyt}|_{z=h}}$; (c) streamwise and (d) vertical velocity standard deviations $\sigma_u = \langle u'u'\rangle_{xyt}^{1/2}$ and $\sigma_w = \langle w'w'\rangle_{xyt}^{1/2}$, scaled by u_*, respectively; (e) opposite correlation coefficient $-r_{uw} = -\langle u'w'\rangle_{xyt}/(\sigma_u\sigma_w)$; (f) streamwise and (g) vertical velocity skewness $Sk_u = \langle u'^3\rangle_{xyt}/\sigma_u^3$ and $Sk_w = \langle w'^3\rangle_{xyt}/\sigma_w^3$; (h) streamwise and (i) vertical velocity kurtosis $Kr_u = \langle u'^4\rangle_{xyt}/\sigma_u^4$ and $Kr_w = \langle w'^4\rangle_{xyt}/\sigma_w^4$.

Before proceeding to discuss the results of flow statistics, the differences of quantifying vegetation density among the LES and the wind tunnel and flume experiments should be considered. The frontal area index (FAI), which is an alias of LAI but more commonly used in laboratory experiments which simulate plant canopies with cylindrical stalks, is 0.47 in the wind tunnel experiment (Brunet et al. 1994) and ranges from 0.032 to 0.512 in the flume experiment (Poggi et al. 2004). However, these FAI values cannot be directly compared to the LAI values used in our LES in consideration of the following facts: (1) the definitions of

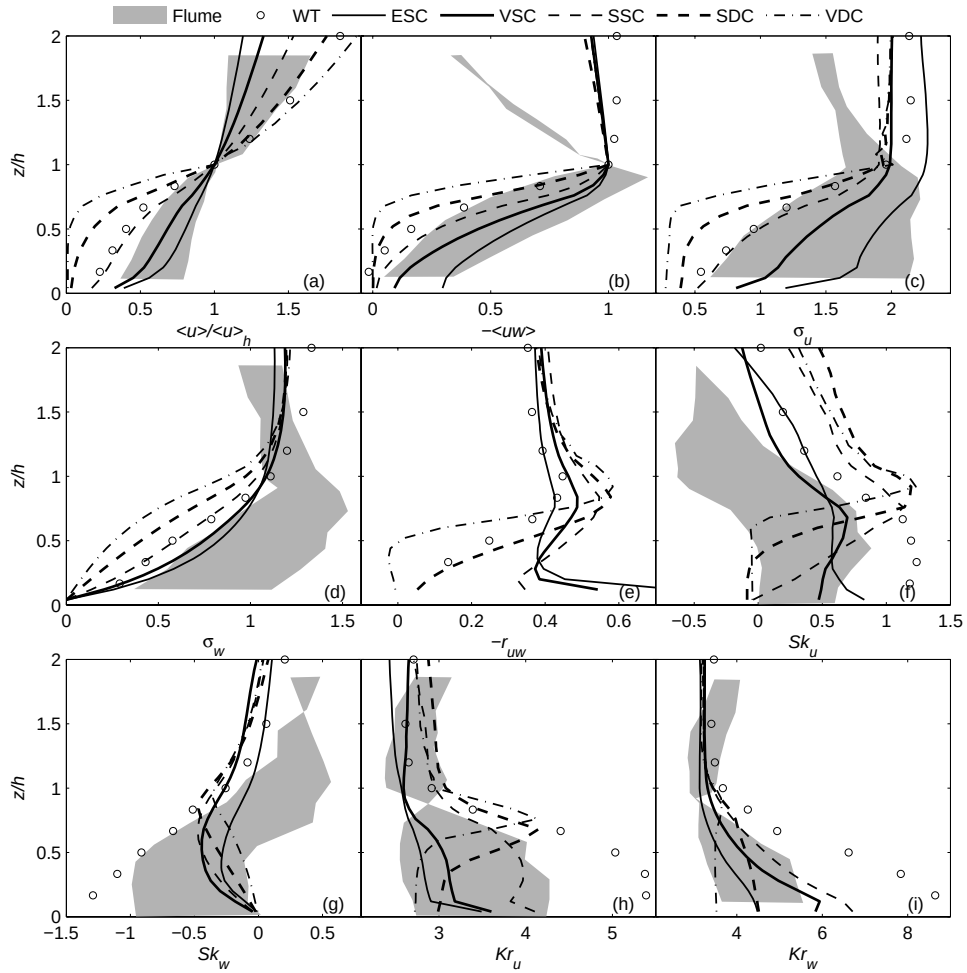

Fig. 2 Vertical profiles of (a) mean streamwise wind velocity; (b) mean shear stress; (c-d) streamwise and vertical velocity standard deviation; (e) uw correlation coefficient; (f-g) streamwise and vertical velocity skewness; (h-i) streamwise and vertical velocity kurtosis for LES simulations with varying LAIs, experimental data measured from flume (Poggi et al. 2004) and wind tunnel (Brunet et al. 1994)

Parameters	C_d	EAI (m^{-1})	FAI	a (m^{-1})	LAI
Wind tunnel	1.35	10	0.47	33.75	1.59
	0.50	0.27	0.032	0.34	0.04
	0.61	0.53	0.064	0.81	0.10
Flume	0.73	1.07	0.129	1.95	0.23
	0.94	2.13	0.256	5.02	0.60
	1.15	4.27	0.512	12.25	1.47

Table 1. Original and normalized parameters in wind tunnel and flume experiments

Property		$\langle u \rangle$ inflection	σ_u / u_*	σ_w / u_*	$-r_{uw}$	$\lvert Sk_u \rvert$	$\lvert Sk_w \rvert$
Surface layer		No	2.5-3.0	1.2-1.3	~0.3	Small	Small
CSL (z=h)	**ESC**	No	2.3	1.1	0.41	0.39	0.07
	CSC	Yes	2.0	1.1	0.46	0.33	0.25
	SSC	Yes	1.9	1.0	0.50	0.78	0.34
	SDC	Yes	1.9	1.0	0.53	1.20	0.39
	VDC	Yes	2.0	0.9	0.57	1.15	0.34
Mixing layer		Yes	1.8	1.4	~0.5	O(1)	O(1)

Table 2. Comparison of statistical flow properties between surface layer, CSL of various LAIs and mixing layer. Values of surface layer and mixing layer are taken from Finnigan (2000)

the drag-force term are different, with the one in flume and wind tunnel having an extra factor of 1/2 (see Eqn. 12 in Brunet et al. 1994; Eqn. 3 in Poggi et al. 2004); (2) The drag coefficient C_d is constant in our LES but it is a function of height in the wind tunnel experiment and a function of height and vegetation density in the flume experiment; (3) The amplitude of C_d is 0.2 in our LES, but in the wind tunnel experiment ranges from less than 1.0 around canopy top to more than 2.0 in the middle of canopy, in the flume experiment ranges from 0.5 to 1.2 for different density settings. Considering the above three points, the values of the element area index (EAI) and FAI in the flume and the wind tunnel experiments can be reconciled to the definitions of a and LAI in the LES, as listed in Table 1. From now on the notations of the parameters are consistent with those used in this study, i.e., a and LAI replace EAI and FAI, respectively. From Table 1 it is clear that the wind tunnel experiment and the densest case of the flume experiments should approximately correspond to the SSC case in the LES, while the sparsest flume experiment should be comparable with the ESC. This conjecture can be verified in observation of Fig. 2. Note that for the flume experiment, the densest canopy set-up corresponds to the left side of the shaded area for $\langle u \rangle_{xyt} / u^h$, $-\langle u'w' \rangle_{xyt} / u_*^2$, σ_u / u_*, σ_w / u_* and Sk_w, but the right side for Sk_u, Kr_u and Kr_w inside canopy. It is vice versa for the sparsest one. Focusing on the level below the canopy top it is possible to see that SSC, wind tunnel experiment and the densest flume experiment share similar values of $\langle u \rangle_{xyt} / u^h$, $-\langle u'w' \rangle_{xyt} / u_*^2$, σ_u / u_* and σ_w / u_* .The shaded areas of the flume experiments basically just cover the cases of ESC, VSC and SSC in all profiles of flow statistics but σ_w / u_* and Sk_w. The discrepancy in σ_w and Sk_w can be partially explained in term of insufficient resolution in the wall region. However, a comparison of the LES results with the statistics reported in Raupach et al. (1996) (c.f. Figure 1 therein), suggest that the simulations are in fair agreement with several experiments filed and laboratory experiment. Close to the ground the amplitudes of the high-order moments of streamwise and vertical velocities (Sk_u, Sk_w, Kr_u and Kr_w) measured in the wind tunnel are greater than those of the LES and flume experiments. This is probably caused by the elasticity of the cylindrical, monofilament nylon fishing line which was used to simulate plant canopy, and can be evidenced from an inspection of the statistics reported in Raupach et al. (1996) (c.f. Figure 1 therein), which shows similarly consistent differences between waving and not waving canopies. Above the canopy top, the profiles vary significantly between the flume and LES/wind tunnel. This is most likely caused by the smaller ratios between boundary layer depth L_z, and h in the flume, but should be not very significant to the present study objectives.

A number of noteworthy features emerge as we focus on the effects of vegetation density on flow statistics. As canopy becomes denser, (1) the inflection of $\langle u \rangle_{xyt} / u^h$ at $z = h$ is stronger; (2) the shear stress and the kinetic energy are damped more rapidly with increasing depth inside canopy; (3) $|r_{uw}|$ increases in the vicinity of canopy top, which means that denser canopy is able to transport momentum more efficiently at the canopy-atmosphere interface; (4) $|Sk_u|$, $|Sk_w|$, Kr_u and Kr_w increase with positive Sk_u and negative Sk_w in the upper part of CSL. This can be interpreted as denser canopies producing more and stronger sweep events. The salient points of these tendencies are summarized in Table 2 and compared with the standard values for a surface layer and a mixing layer taken from Finnigan (2000). This comparison of single-point turbulence statistics clearly demonstrates that the overall behaviors of ESC resemble a SL while those of SDC and VDC are in accordance with a PML. VSC and SSC are affected by both the potential mechanisms of SL and PML, and thus the values of their statistics are between the two flow types.

4.2 *One-dimensional turbulent structures*

Because the first POD mode statistically carries the most percentage of TKE over an ensemble of turbulent field, this energetic pattern has been treated as 'coherent structure' or 'characteristic eddy' in a number of applications, such as channel flow (Moin and Moser 1989), PML (Delville et al. 1999), CSL (Finnigan and Shaw 2000). Finnigan and Shaw (2000) analyzed the same set of data as in Brunet et al. (1994) and showed the geometries of coherent structures based on one-dimensional and multi-dimensional POD analysis. One-dimensional analysis found that the first of 42 modes takes approximately 53 percent of the total energy of $\langle u'^2 + w'^2 \rangle$ and the first five modes capture up to about 82 percent.

The first three one-dimensional POD modes of SSC are compared with those in Finnigan and Shaw (2000) in Fig. 3 since the normalized LAI of wind tunnel experiment is close to that of SSC. The same procedures are followed: (1) only u and w are combined to form the two-point correlation tensor; (2) The square root of the eigenvalues $\lambda^{(m)}$ are multiplied to the corresponding eigenfunctions $\phi^{(m)}$ so that the amplitudes of all the modes are comparable. The signs of eigenfunctions are set consistent between LES and wind tunnel although it is undeterminable from the eigen problem of POD. Also all the modes of the wind tunnel results are scaled by friction velocity ($u_*^{WT} = 0.87 m/s$) as it performed in our LES. The general patterns of the one-dimensional modes from both studies are in a good agreement, which appear as: (1) the same relative signs

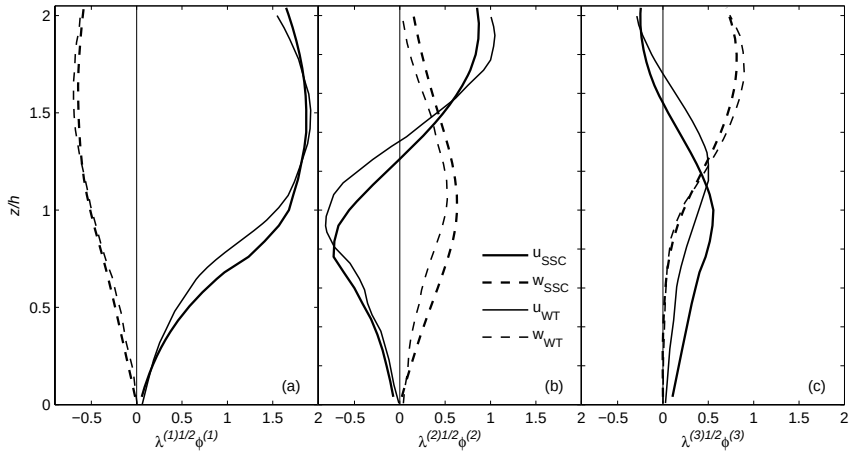

Fig. 3. Comparison of the first three normalized one-dimensional eigenfunctions $\lambda^{(i)1/2}\phi^{(i)}$ between LES SSC and wind tunnel experiment

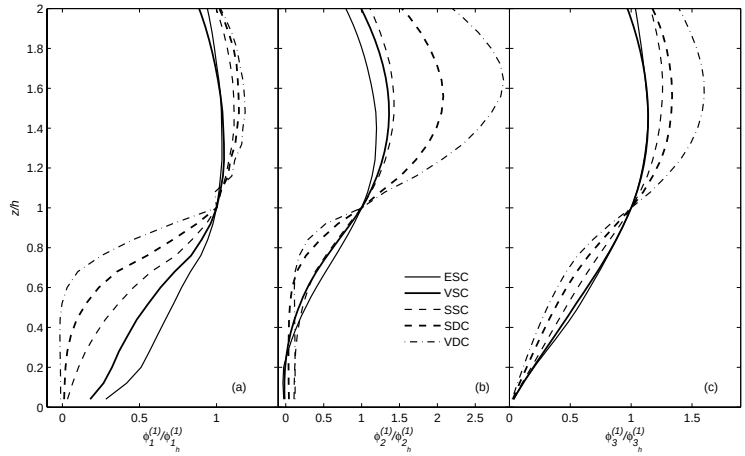

Fig. 4 Comparison of the first eigenfunctions of (a) u ; (b) v ; and (c) w for canopies of five different LAIs

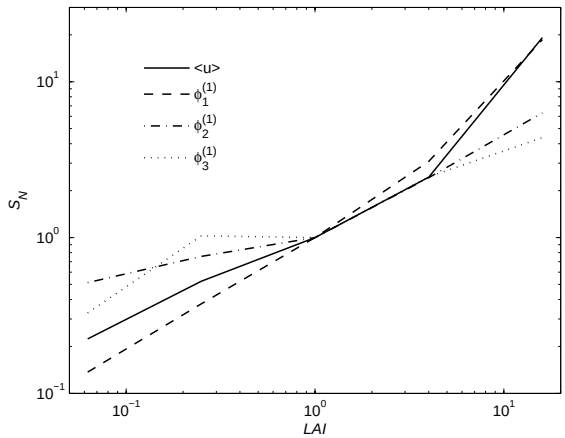

Fig. 5 Normalized strength of inflection S_N versus LAI for $< u >$, $\phi_1^{(1)}$, $\phi_2^{(1)}$ and $\phi_3^{(1)}$

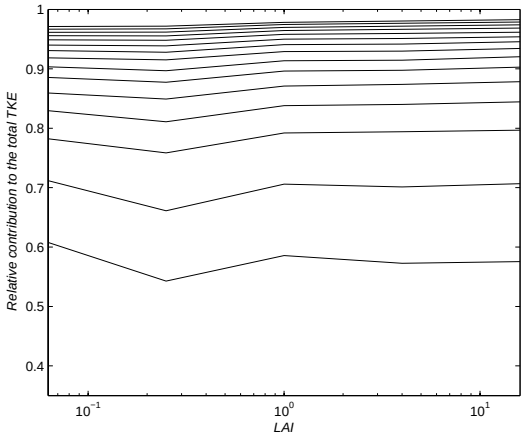

Fig. 6 Cumulative contribution of the first fifteen eigen modes to the total energy of $u^2 + w^2$ versus LAI. The number of the modes increases from bottom to top

of u and w modes; (2) close amplitudes in all six comparisons of single lines; (3) close zero-crossings and similar vertical trends. The compelling match of this comparison shows that our LES is able to produce the similar canopy turbulence as in wind tunnel experiments with vegetation of close density values. There is also a discrepancy in this comparison: the elevations where all the POD modes $\lambda^{(m)1/2}\phi^{(m)}$ peak are higher in wind tunnel than in LES, and this difference is more pronounced for u than for w. This happens because the vegetation density in LES is not exactly uniformly distributed as in wind tunnel. The damping layer in the upper part of canopy absorbs less momentum than the canopy top in wind tunnel experiments, and consequently causes coherent large structures behave differently. This discrepancy in elevations is reduced (not shown here) if the vertical stand of LES is scaled by the lower part of the canopy rather than the entire canopy height h.

We furthermore explore the effects of canopy vegetation density on the one-dimensional energetic structures. In Fig. 4, these structures of canopies with five different LAIs are normalized by their values at $z=h$ as $\phi_i^{(m)}/\phi_{ih}^{(m)}$. This scaling facilitates comparing the strength of inflections at canopy top. The structures of denser canopies have stronger inflection for all cases with the u structure showing more pronounced inflection than those of v and w. As a quantitative measure of inflection strength the square of the second derivative of a vertical profile $p(z)$ is integrated over $[0.6h,1.4h]$, $S^p=\int_{0.6h}^{1.4h}|p''(z)|^2dz$. Here the choice of the range of integration is somewhat arbitrary. However, the results are similar for other reasonable ranges. S^p is then normalized by its value at the case of SSC since we are not interested in the absolute amplitude of S^p, i.e. $S_N^p(LAI)=S^p(LAI)/S^p(1)$. $S_N^p(LAI)$ is computed for the streamwise mean velocity profile $\langle u\rangle_{xyt}$ and the first POD modes $\phi_i^{(1)}$ and plotted using log-log scaling in Fig. 5. S_N generally increases as LAI increases except for $S_N^{\phi_3^{(1)}}$, which slightly decreases from VSC to SSC. Compared with $\langle u\rangle_{xyt}$ and $\phi_1^{(1)}$, the weaker effect of LAI on $\phi_{2,3}^{(1)}$ are indicated by smaller values of S_N. Additionally, $S_N^{\langle u\rangle_{xyt}}$ and $S_N^{\phi_1^{(1)}}$ approximately follow a power-law relationship as a function of LAI with an exponent of 0.75. The effect of vegetation density on the convergence rate of eigenvalue series is also studied. This measure normally serves as an indicator of the relative importance of the first or the first few modes in terms of their capability of carrying kinetic energy. Based on Fig. 6, it is found that LAI does not have a significant influence on convergence rates while the LES results are definitely consistent with the wind tunnel one in Finnigan and Shaw (2000); In the wind tunnel experiments, the first mode takes approximately 53 percent and the first five modes capture up to 82 percent of the total energy of u^2+w^2. In the LES results, the percentage of the first mode ranges from 54 percent (VSC) to 61 percent (ESC), and that of the first five modes is between 85 to 86 percent.

4.3 *Multi-dimensional turbulent structures*

The POD analysis is extended to multi-dimensional space. What needs to be noted is that the POD technique itself is incapable of determining the sign of eigenmodes due to its nature of optimizing the second order moment. However, the issue of sign can be addressed by reconciling the dominance of sweep/ejection motions of coherent structure with that of the instantaneous turbulent field (Huang et al. In Preparation) or implementing the phase recovery algorithm of three-point correlation (Moin and Moser 1989). In the present paper, the method of the sweep/ejection dominance is adopted.

We first conduct two-dimensional analysis in the $x-z$ plane. Precedent field and laboratory experiments have painted a consistent picture of turbulent structures in CSL in the steamwise-vertical plane (e.g. Gao et al. 1989; Gardiner 1994; Finnigan and Shaw 2000), which can be characterized as (1) intermittent occurrences of strong sweep motions and relatively weak ejection events; (2) stronger ejections and weaker sweeps with height. In Fig. 7, large-scale coherent structures in the $x-z$ plane are educed using POD and the compactness condition to recover phase angles (e.g. Moin and Moser 1989; Finnigan and Shaw 2000). The most apparent feature through the observation of Fig. 7 (a, c, e) is the dominance of strong sweep motions. These energetic structures almost occupy the whole plot area with the significant parts occurring in the range of $r_x/h\subset[-2,2]$. Vertically, the strength of sweep motions peaks in the range of $z/h\subset[0.8,1.5]$ and decrease gradually above, which agrees well with available findings (Finnigan and Shaw 2000). In Fig. 7, it is not possible to explicitly observe ejection structures and the reason is that the first POD mode ignores less energetic patterns. The main effect of vegetation density on this two-dimensional structure is the uplift of the structure as the canopy becomes denser, and consequently, the lower and middle levels of the canopy are filled by relatively weak flows. In reality there is an interesting pattern hidden inside the canopy ranging from $-2h$ to 0 streamwisely. This pattern can be clearly observed from the zoom-in and magnified pictures in (b, d, f), which correspond to their counterparts on the left, respectively. What we can see from (b) is only a swarm of sweeps occupying the whole zoom-in area; but in (d) a clockwise-rotating vortex emerges up with its center approximately positioned at $[-1.2h,0.25h]$ and in (f) this vortex moves upward and towards the right direction with the center located at $[-0.8h,0.65h]$. The case of

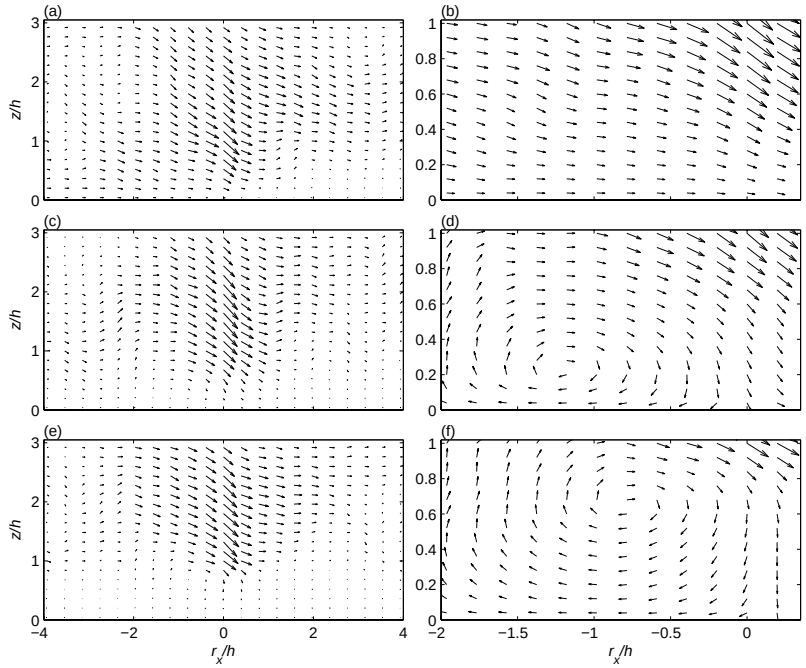

Fig. 7 $u - w$ vector plot of two-dimensional turbulent structure in the $x - z$ plane for (a) ESC, (c) SSC and (e) VDC. (b,d,f) are their corresponding zoom-in and magnified version

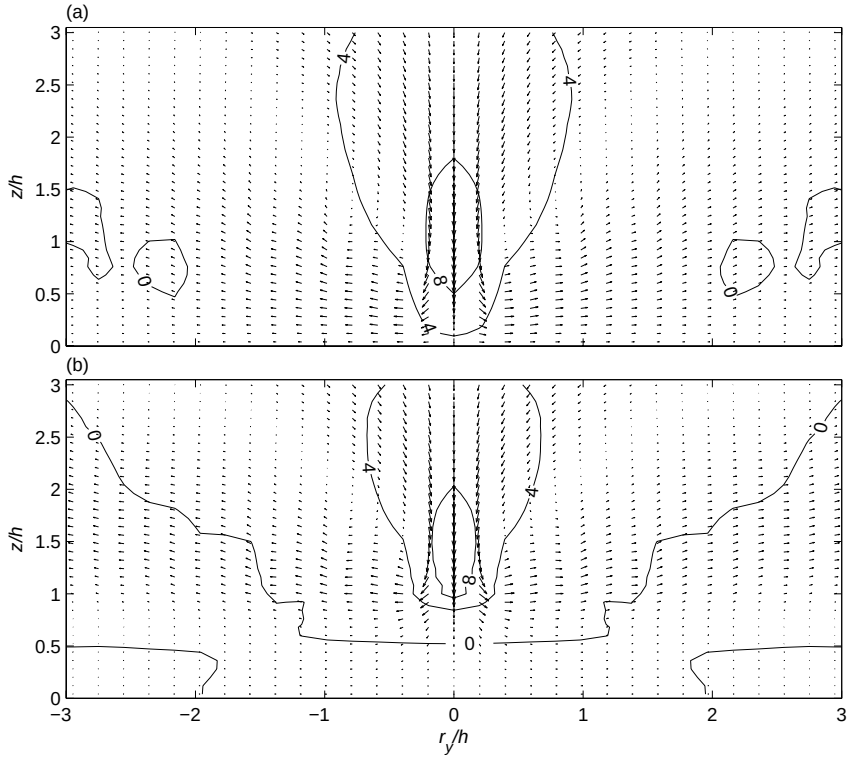

Fig. 8 $v - w$ vector plot with u contour of two-dimensional turbulent structure in the $y - z$ plane for (a) ESC and (b) VDC

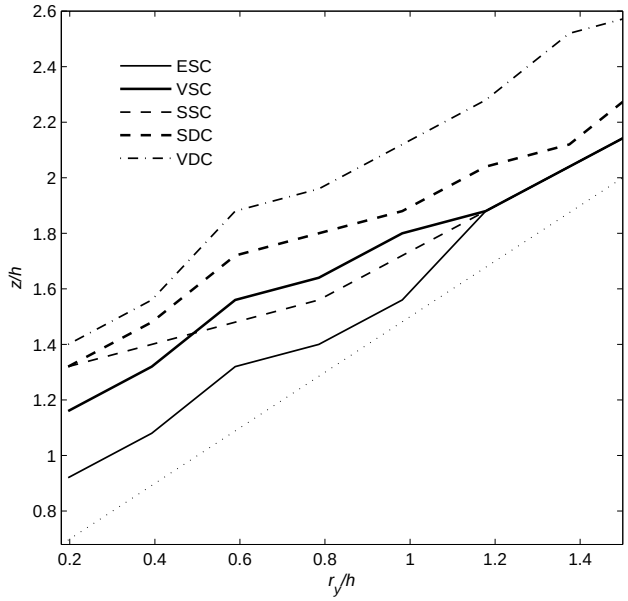

Fig. 9 Height of zero crossings of v in the $y-z$ plane turbulent structure versus r_y for varying LAIs. The straight line with an angle of 45° is plotted for reference

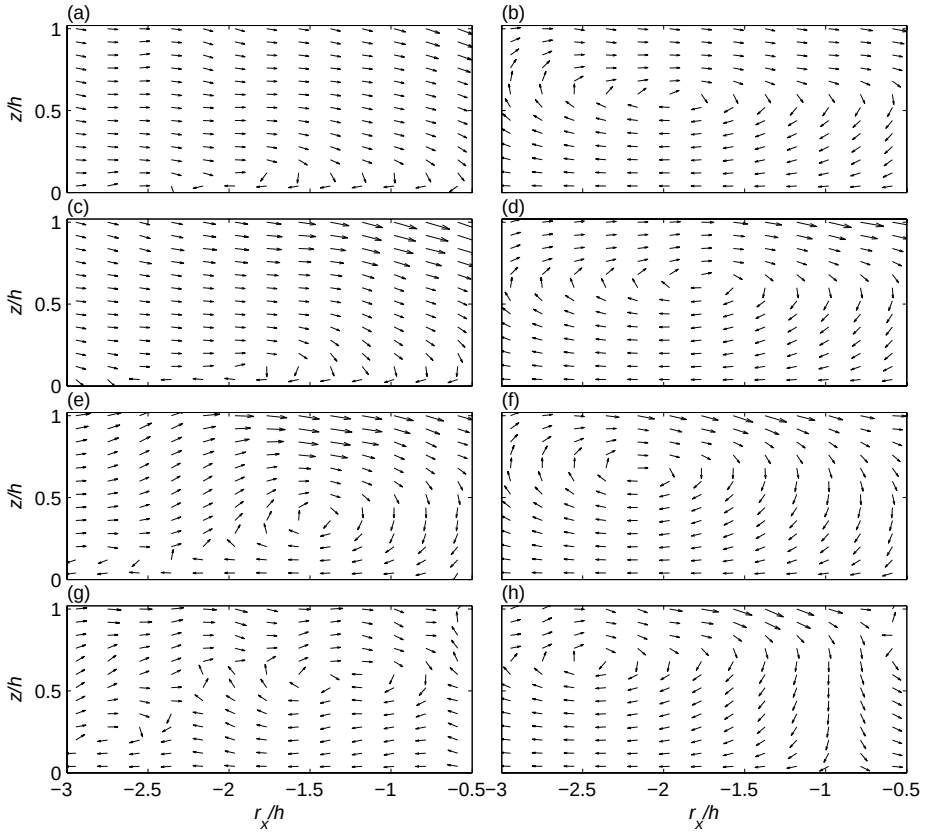

Fig. 10 $u-w$ velocity vectors of three-dimensional turbulent structure projected onto the $x-z$ plane for SSC (a, c, e, g) and VDC (b, d, f, h) at $r_y/h=0$ (a, b), $r_y/h=0.4$ (c, d), $r_y/h=0.8$ (e, f) and $r_y/h=1.2$ (g, h), respectively

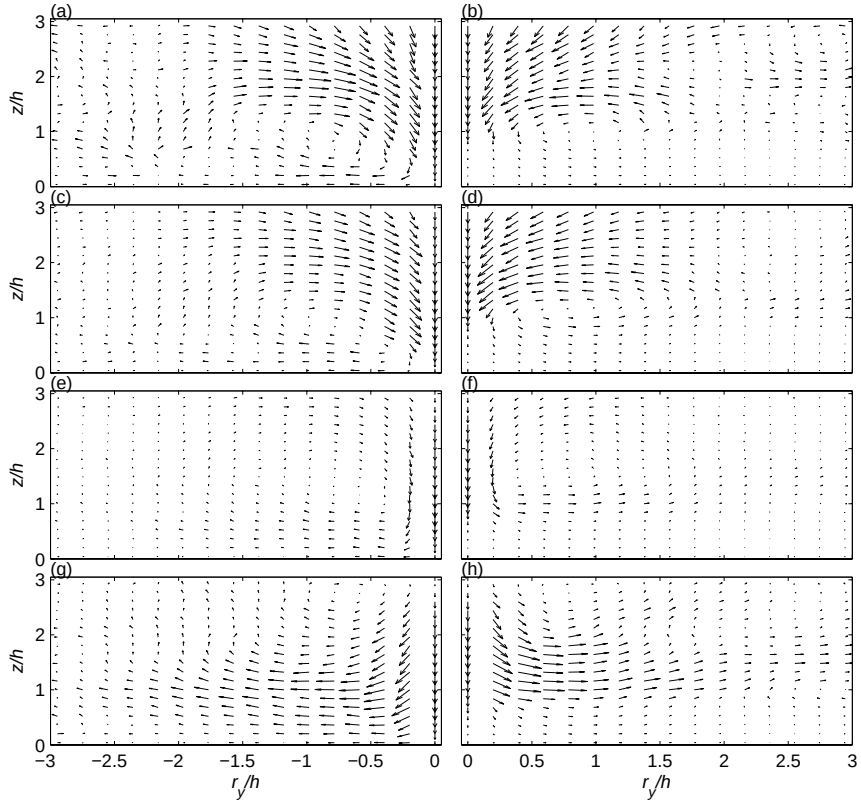

Fig. 11 $v-w$ velocity vectors of three-dimensional turbulent structure projected onto the $y-z$ plane for ESC (a, c, e, g) and VDC (b, d, f, h) at $r_x/h=-0.8$ (a, b), $r_x/h=-0.4$ (c, d), $r_x/h=0$ (e, f) and $r_x/h=0.4$ (g, h), respectively

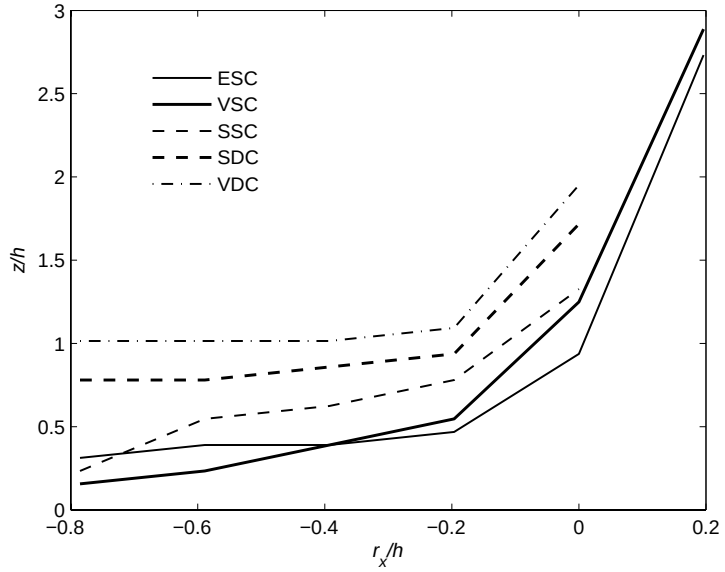

Fig. 12 Heights of v zero-crossings of three-dimensional turbulent structure at $r_y/h=0.4$ against r_x/h for canopies of varying LAIs

SDC was also checked (not shown here) and a similar vortex was found with its center consistently located between those of SSC and VDC. It is clear that if and where this type of vortex can be formed is related to LAI and then the ability of the canopy of absorbing momentum: the vortex is not formed in the cases of ESC and VSC; however, as the canopy goes denser from SSC to VDC, the vortex is formed and its center approaches closer to the canopy top. The wind tunnel in Finnigan and Shaw (2000) has a LAI close to SSC, but this type of vortex was not found in the two-dimensional analysis (c.f. Fig. 9 in Finnigan and Shaw 2000), which is probably due to the insufficient vertical sampling resolution in the measurement procedure. The mechanism controlling the generation of this vortex is unclear at this point, but this fact can not be explained by the Kelvin-Helmholtz instability theory because the vortices controlled by this instability should be vertically centered around the position where the vertical gradient of the mean streamwise velocity and the stress peak, i.e., the canopy top, and the vortices in Fig. 7 are all considerably far from the canopy top. In fact, this type of structure can be discerned in previous field studies (c.f. Fig. 5-6 in Gao et al. 1989).

The two-dimensional structure in the $y-z$ plane has been investigated more extensively than that in the $x-z$ plane. This structure takes similar form within channel flow, ABL, PML and CSL (Moin and Moser 1989; Delville et al. 1999; Finnigan and Shaw 2000; Huang et al. In Preparation), consisting of a pair of counter-rotating vortices and a strong sweep or ejection motion. Within channel flow and ABL, the dominant motion is ejection while within CSL sweep dominates ejection. In Fig. 8, this structure of vortex pair is plotted for ESC and VDC. The iso- lines of u as well as the vortex pair are moved up and compressed as it goes from ESC to VDC. This is in good agreement with the elevation of spanwise vortex in Fig. 8. The heights of zero-crossings of v are reported in Fig. 9 for canopies with five different LAIs. Except that the cases of VSC and SSC are entangled for $r_y/h > 0.5$, which may be caused by the insufficient resolution in the LES, this scenario shows the trend that large-scale structure in the $y-z$ plane moves up as vegetation density increases. Also, the center locations of vortex pair appears to incline at an angle of approximately 45°, which is the same as what was found with ABL (Huang et al. In Preparation).

Three-dimensional coherent structures are also obtained for our simulations data. To our knowledge this is the first attempt to show the three-dimensional geometry of the non-conceptual turbulent coherent structures within CSL. In Fig. 10, $u-w$ vectors of $x-z$ plane slices are projected at $r_y/h = \{0, 0.4, 0.8, 1.2\}$ for the cases of SSC and VDC, respectively. Vectors of small amplitudes are magnified so that their directions can be clearly observed. Clockwise-rotating vortex is consistently found in accordance with the two-dimensional version. In the case of SSC, this type of vortex develops from a strong vertical u gradient close to ground at $r_y/h = 0$ (Fig. 10a), and then ascends to around $z/h = 0.55$ at $r_y/h = 1.2$. This tendency of ascending of the spanwise vortex is less significant for the case of VDC, with the center of the vortex moving up approximately from $z/h = 0.55$ for $r_y/h = 0$ to $z/h = 0.7$ for $r_y/h = 1.2$. In Fig. 11, $v-w$ velocity vectors on $y-z$ plane slices of the three-dimensional coherent structures are also shown. The vectors are plotted for $r_x/h = \{-0.8, -0.4, 0, 0.4\}$ and for the cases of ESC (left) and VDC (right), respectively. Since coherent structures in the $y-z$ plane are symmetric with respect to $r_y/h = 0$, vector plots are showed for only half plane in r_y. The results are similar with their counterparts within channel flow (Moin and Moser 1989) and ABL (Huang et al. In Preparation) with the counter-rotating vortex pairs all moving up along x. Comparing VDC and ESC, all vortices rotate much higher in VDC at the same location r_x.

The effect of vegetation density on the elevation of three-dimensional coherent structure is quantified in Fig. 12, where heights of zero-crossings of v are plotted versus r_x/h for the five densities. The spanwise position $r_y/h = 0.4$ is used to obtain these results but other reasonable alternatives produce similar results. The three-dimensional structures curve up in all five cases. The angle of inclination can increase, taking the example of ESC, from 0° in the range of $r_x/h \subset [-0.6, -0.4]$, to 84° in $r_x/h \subset [0, 0.2]$. Greater vegetation density is clearly prone to cause higher elevation of this structure although the cases of ESC and VSC are slightly entangled upstream of $r_x/h = -0.4$. For instance, at $r_x/h = -0.2$ the ESC structure is elevated approximately at $z/h = 0.4$; however, this value is 0.5, 0.75, 0.9 and 1 for VSC, SSC, SDC and VDC, respectively.

5 CONCLUSIONS

The effects of vegetation density on basic flow statistics and turbulent structures are systematically investigated by using LES simulate canopy turbulence. The following conclusions can be made on the basis of our simulation and analysis:

1. Our LES is able to produce similar turbulent dynamics within CSL as in wind tunnel experiment (Finnigan and Shaw 2000) based on the results of comparison on flow statistics and one-dimensional turbulent structures: (i) vertical profiles of $\langle u \rangle_{xyt}/u^h$, $-\langle u'w' \rangle/u_*^2$, σ_u and σ_w of SSC inside canopy are all close to those of wind tunnel and flume experiments with similar LAI values; (ii) One-dimensional POD eigenfunctions of SSC and the convergence rate of

eigenvalues fit well with those of wind tunnel measurements.

2. Denser canopy generally causes stronger inflection of $\langle u \rangle_{xyt}$ and vertical turbulent structures at canopy top, faster decreases of shear stress and TKE in the upper part of canopy, stronger correlation of u and w around $z = h$ and greater Sk_u and Sk_w around $z = h$ and above.

3. Turbulent structure in the $x - z$ plane is dominated by strong sweeps, consistent with what was found through wind tunnel experiments. Clockwise-rotating vortex, which is caused by the damping effects of momentum of canopies, is also observed for relatively dense canopies (SSC, SDC and VDC) and the center position moves up from $0.25h$ to $0.65h$ as canopy becomes denser.

4. Turbulent structure in the $y - z$ plane is composed of a counter-rotating spanwise vortex pair and a strong sweep motion between the vortex pair, which agrees with wind tunnel result. Furthermore, the center of the vortex is showed to incline at an angle of approximately 45^o along y, which is the same as in ABL (Huang et al. In Preparation).

5. Along the streamwise direction, the spanwise vortex pair curves up with the inclination angle ranging between 0^o to 84^o. Turbulent structures tend to be more elevated as the vegetation density of canopy increases.

6 ACKNOWLEDGEMENTS

This material is based upon work supported by the Department of Energy Southeastern Regional Center of the National Institute for Climate Change Research, grant number DE-FC02-06ER64156.

7 REFERENCES

Albertson JD (1996) Large-eddy simulation of land-atmosphere interaction. PhD Thesis, University of California Davis.

Albertson JD, Katul GG and Wiberg P (2001) Relative importance of local and regional controls on coupled water, carbon, and energy fluxes. Advances in Water Resources. 24:1103-1118.

Albertson JD and Parlange MB (1999a) Natural integration of scalar fluxes from complex terrain. Advances in Water Resources. 23:239-252.

Albertson JD and Parlange MB (1999b) Surface length scales and shear stress: Implications for land-atmosphere interaction over complex terrain. Water Resour Res. 35:2121-2132.

Asner GP, Jonathan MO and Hicke JA (2003) Global synthesis of leaf area index obervations: implications for ecological and remote sensing studies. Global Ecol Biogeogr. 12:191-205.

Berkooz G, Holmes P and Lumley JL (1993) The proper orthogonal decomposition in the analysis of turbulent flows. Ann Rev Fluid Mech. 25:539-575.

Brunet Y, Finnigan JJ and Raupach MR (1994) A Wind-Tunnel Study of Air-Flow in Waving Wheat - Single-Point Velocity Statistics. Boundary-Layer Meteorol. 70:95-132.

Cassiani M, Katul GG and Albertson JD (2008) The effects of canopy leaf area index on airflow across forest edges: large-eddy simulation and analytical results. Boundary-Layer Meteorol. accepted.

Deardorff JW (1972) Numerical investigations of neutral and unstable planetary boundary layers. J Atmos Sci. 29:91-115.

Delville J, Ukeiley L, Cordier L, Bonnet JP and Glauser M (1999) Examination of large-scale structures in a turbulent plane mixing layer. Part 1. Proper orthogonal decomposition. J Fluid Mech. 391:91-122.

Dwyer MJ, Patton EG and Shaw RH (1997) Turbulent kinetic energy budgets from a large-eddy simulation of airflow above and within a forest canopy. Boundary-Layer Meteorol. 84:23-43.

Finnigan J (2000) Turbulence in plant canopies. Annual Review of Fluid Mechanics. 32:519-571.

Finnigan JJ and Shaw RH (2000) A wind-tunnel study of airflow in waving wheat: An EOF analysis of the structure of the large-eddy motion. Boundary-Layer Meteorol. 96:211-255.

Gao W, Shaw RH and Paw KT (1989) Observation of Organized Structure in Turbulent-Flow within and above a Forest Canopy. Boundary-Layer Meteorol. 47:349-377.

Gardiner BA (1994) Wind and Wind Forces in a Plantation Spruce Forest. Boundary-Layer Meteorol. 67:161-186.

Holmes P, Lumley JL and Berkooz G (1996) Turbulence, coherent structures, dynamical systems, and symmetry. Cambridge University Press, New York.

Huang J, Cassiani M and Albertson JD (In Preparation) Analysis of coherent structures within atmospheric boundary layer: comparison between LES and DNS. Boundary-Layer Meteorol.

Katul GG and Albertson JD (1998) An investigation of higher-order closure models for a forested canopy. Boundary-Layer Meteorol. 89:47-74.

Kosovic B (1997) Subgrid-scale modelling for the large-eddy simulation of high-Reynolds-number boundary layers. J Fluid Mech. 336:151-182.

Lumley JL (1967) The structure of inhomogeneous turbulent flows. In: Yagolm AM and Tatarsky VI (eds). Atmospheric Turbulence and Radio Wave Propagation, Moscow1967, / Nauka, City, pp. 166-178.

Lumley JL (1970) Stochastic tools in turbulence. Academic Press, New York,.

Lumley JL (1981) Coherent structures in turbulence. In: Meyer RE (ed). Transition and Turbulence1981, / Academic, City, pp. 215-241.

Mason PJ and Thomson DJ (1992) Stochastic Backscatter in Large-Eddy Simulations of Boundary-Layers. J Fluid Mech. 242:51-78.

Moeng CH (1984) A Large-Eddy-Simulation Model for the Study of Planetary Boundary-Layer Turbulence. Journal of the Atmospheric Sciences. 41:2052-2062.

Moin P and Moser RD (1989) Characteristic-Eddy Decomposition of Turbulence in a Channel. J Fluid Mech. 200:471-509.

Novak MD, Warland JS, Orchansky AL, Ketler R and Green S (2000) Wind tunnel and field measurements of turbulent flow in forests. Part I: Uniformly thinned stands. Boundary-Layer Meteorol. 95:457-495.

Patton EG, Davis KJ, Barth MC and Sullivan PP (2001) Decaying scalars emitted by a forest canopy: A numerical study. Boundary-Layer Meteorol. 100:91-129.

Poggi D, Porporato A, Ridolfi L, Albertson JD and Katul GG (2004) The effect of vegetation density on canopy sub-layer turbulence. Boundary-Layer Meteorol. 111:565-587.

Porte-Agel F, Meneveau C and Parlange MB (2000) A scale-dependent dynamic model for large-eddy simulation: application to a neutral atmospheric boundary layer. J Fluid Mech. 415:261-284.

Raupach MR, Finnigan JJ and Brunet Y (1996) Coherent eddies and turbulence in vegetation canopies: The mixing-layer analogy. Boundary-Layer Meteorol. 78:351-382.

Schmidt H and Schumann U (1989) Coherent Structure of the Convective Boundary-Layer Derived from Large-Eddy Simulations. J Fluid Mech. 200:511-562.

Shaw RH and Schumann U (1992) Large-Eddy Simulation of Turbulent-Flow above and within a Forest. Boundary-Layer Meteorol. 61:47-64.

Shen SH and Leclerc MY (1997) Modelling the turbulence structure in the canopy layer. Agricultural and Forest Meteorology. 87:3-25.

Sirovich L (1987a) Turbulence and the Dynamics of Coherent Structures .1. Coherent Structures. Quart Appl Math. 45:561-571.

Sirovich L (1987b) Turbulence and the Dynamics of Coherent Structures .2. Symmetries and Transformations. Quart Appl Math. 45:573-582.

Sirovich L (1987c) Turbulence and the Dynamics of Coherent Structures .3. Dynamics and Scaling. Quart Appl Math. 45:583-590.

Su HB, Shaw RH and Paw U KT (2000) Two-point correlation analysis of neutrally stratified flow within and above a forest from large-eddy simulation. Boundary-Layer Meteorol. 94:423-460.

Su HB, Shaw RH, U KTP, Moeng CH and Sullivan PP (1998) Turbulent statistics of neutrally stratified flow within and above a sparse forest from large-eddy simulation and field observations. Boundary-Layer Meteorol. 88:363-397.

Sullivan PP, McWilliams JC and Moeng CH (1996) A grid nesting method for large-eddy simulation of planetary boundary-layer flows. Boundary-Layer Meteorol. 80:167-202.

Yang B, Morse AP, Shaw RH and Paw U KT (2006a) Large-eddy simulation of turbulent flow across a forest edge. Part II: Momentum and turbulent kinetic energy budgets. Boundary-Layer Meteorol. 121:433-457.

Yang B, Raupach MR, Shaw RH, Tha K, Paw U and Morse AP (2006b) Large-eddy simulation of turbulent flow across a forest edge. Part I: Flow statistics. Boundary-Layer Meteorol. 120:377-412.